View Article Online / Journal Homepage / Table of Contents for this issue
Dynamic Article Links

PCCP

Cite this: *Phys. Chem. Chem. Phys.*, 2012, **14**, 11974–11980

www.rsc.org/pccp

PAPER

Published on 03 July 2012. Downloaded by Technische Informationsbibliothek (TIB) on 26/10/2017 14:16:50.

Extremely slow Li ion dynamics in monoclinic Li_2TiO_3—probing macroscopic jump diffusion *via* ^{7}Li NMR stimulated echoes

Benjamin Ruprecht,*[a] Martin Wilkening,†[a] Reinhard Uecker[b] and Paul Heitjans[a]

Received 22nd May 2012, Accepted 3rd July 2012
DOI: 10.1039/c2cp41662j

A thorough understanding of ion dynamics in solids, which is a vital topic in modern materials and energy research, requires the investigation of diffusion properties on a preferably large dynamic range by complementary techniques. Here, a polycrystalline sample of Li_2TiO_3 was used as a model substance to study Li motion by both ^{7}Li spin-alignment echo (SAE) nuclear magnetic resonance (NMR) and ac-conductivity measurements. Although the two methods do probe Li dynamics in quite different ways, good agreement was found so that the Li diffusion parameters, such as jump rates and the activation energy, could be precisely determined over a dynamic range of approximately eleven decades. For example, Li solid-state diffusion coefficients D_σ deduced from impedance spectroscopy range from 10^{-23} m^2 s^{-1} to 10^{-12} m^2 s^{-1} (240–835 K). These values are in perfect agreement with the coefficients D_{SAE} deduced from SAE NMR spectroscopy. As an example, $D_{SAE} = 2 \times 10^{-17}$ m^2 s^{-1} at 433 K and the corresponding activation energy determined by NMR amounts to 0.77(2) eV (400–600 K). At room temperature D_σ takes a value of 3×10^{-21} m^2 s^{-1}.

1 Introduction

The microscopic study of ion hopping processes in crystalline materials is a key research area in the field of solid state ionics. In particular, the investigation of lithium ion dynamics in materials being relevant for energy storage systems such as rechargeable lithium-ion batteries is currently of utmost interest.[1–6] A comprehensive understanding of ion dynamics requires studying transport parameters over wide scales in space and time, *i.e.*, by the use of complementary techniques being sensitive to ion motions on different length scales.[7,8] Prior to the application of (newly established) sophisticated techniques to study dynamics in complex, application-oriented materials, from a fundamental point of view it is highly useful to begin with the investigation of suitable model substances. This enables the evaluation of experimental findings with respect to the well-defined structural properties of model compounds. It helps develop a readily comprehensible and coherent interpretation which can later be used to understand the results obtained from non-model systems.

In the present paper, monoclinic (phase pure) Li_2TiO_3 served as such a model substance to study Li ion dynamics by both ^{7}Li spin-alignment echo (SAE) NMR and impedance spectroscopy (IS). The two methods, when taken together, are sensitive to Li motions in a dynamic range covering many decades. While IS has been used to determine Li transport parameters since many decades,[9–11] SAE NMR spectroscopy has been applied to Li ion conductors just in the last ten years.[8,12–28] Originally, the method was developed by Spiess and co-workers to gather both dynamic and geometric information on the translational and rotational processes of deuterons.[29–33] As we have pointed out quite recently, when applied to Li ion conductors, SAE NMR is sensitive to slow, long-range Li diffusion processes although the corresponding jump rates are probed from an atomic-scale point of view.[8,28] Hence, results extracted from variable-temperature stimulated echoes are predisposed to be compared with dc-conductivity values reflecting the charge carrier transport through successful ion jump processes occurring on approximately the millisecond time scale.

The (monoclinic) β-modification of Li_2TiO_3, reported to be isostructural to Li_2SnO_3,[34] is one of the three known polymorphs of Li_2TiO_3.[35,36] Besides its potential use as an additive in lithium-ion batteries,[37,38] β-Li_2TiO_3 is discussed to serve as a blanket material for tritium breeding in deuterium–tritium fusion reactors.[39–43] While the layer-structured β-form reversibly transforms into a cubic γ-modification at temperatures higher than approximately 1425 K,[44] the third modification, *viz* an NaCl-type thermodynamically metastable α-phase with cubic symmetry, undergoes a phase transformation into the β-polymorph at $T > 575$ K.[45]

[a] *Leibniz University Hannover, Institute of Physical Chemistry and Electrochemistry, and ZFM – Center for Solid State Chemistry and New Materials, Callinstr. 3a, 30167 Hannover, Germany. E-mail: heitjans@pci.uni-hannover.de, ruprecht@pci.uni-hannover.de; Fax: +49 511 762 19121; Tel: +49 511 762 3185*
[b] *Leibniz Institute for Crystal Growth (Forschungsverbund Berlin e.V.), Max-Born-Str. 2, 12489 Berlin, Germany*
† Present address: Graz University of Technology, Institute for Chemistry and Technology of Materials, Stremayrgasse 9, 8010 Graz, Austria. E-mail: wilkening@tugraz.at, Fax: +43 316 873 1032330; Tel: +43 316 873 32330.

 This journal is © the Owner Societies 2012

View Article Online

Published on 03 July 2012. Downloaded by Technische Informationsbibliothek (TIB) on 26/10/2017 14:16:50.

Li conductivity in β-Li_2TiO_3 is reported to be extremely low.[46] At 573 K the dc conductivity σ_{dc} amounts to approximately 3×10^{-6} S cm^{-1};[47] the corresponding activation energies $E_{a,\sigma}$ range from 0.6 to 1.1 eV depending on the stoichiometry of the samples studied.[46,48] Hence, in the temperature range from 300 to 500 K, Li jump rates ranging from 1 s^{-1} to 10^4 s^{-1} are expected. These values match the dynamic window in which SAE NMR is sensitive enabling a direct comparison of the results obtained from the two methods.

Quite recently, Li dynamics in β-Li_2TiO_3 have been investigated by both molecular dynamics simulations and ^{7}Li SAE NMR.[49] However, the NMR measurements carried out seem to be affected by a rather large non-diffusive background contribution which, in many cases, make it very difficult to directly extract Li jump rates and, thus, an activation energy. Vijayakumar *et al.*[49] reported an activation energy probed by stimulated echo NMR which is lower compared to the values[46] commonly deduced from dc-conductivity measurements on β-Li_2TiO_3. In the present study, we will carefully compare the recently presented results[49] with our own findings on a sample which has been prepared from a highly pure melt of Li_2TiO_3.

2 Experimental details

Phase pure β-Li_2TiO_3 was obtained by crystallizing the corresponding melt in a Pt crucible at room temperature yielding a polycrystalline sample which was characterized by X-ray powder diffraction (XRD). Sharp XRD peaks indicate mean crystallite sizes with diameters in the μm range. For the subsequent temperature-dependent NMR measurements the sample was fire-sealed in a quartz ampoule (5 mm to 8 mm in outer diameter, 3.5 cm to 4.5 cm in length) under vacuum. Prior to the conductivity measurements the powder samples were uniaxially cold-pressed at 1 GPa to cylindrical pellets which were 8 mm in diameter and approximately 1 mm in thickness. Electrodes were applied to the non-sintered pellets by Au evaporation. For the measurements carried out at higher temperatures Pt electrodes have been used.

2.1 NMR measurements

^{7}Li NMR measurements were carried out using a modified MSL 100 spectrometer (equipped with a Kalmus 400 W amplifier) as well as an MSL 400 (Bruker) spectrometer. While the MSL 100 is connected to a field-variable Oxford cryomagnet with a nominal field of 4.8 T, the MSL 400 NMR spectrometer is used in combination with a 9.4 T magnet. The corresponding ^{7}Li NMR resonance frequencies were 77.7 MHz and 155.5 MHz, respectively. Depending on the temperature range, commercial probes and home-built (high-temperature) probes were used to record ^{7}Li NMR spin–lattice relaxation (SLR) rates[50] as well as ^{7}Li NMR spin-alignment echoes.[16,23,51,52] The temperature in the sample chamber was monitored using a Ni–CrNi-thermocouple in connection with an Oxford intelligent temperature controller (ITC 4). Low temperatures were achieved by a stream of freshly evaporated air. The high-temperature probe is equipped with a bifilar heating coil.

^{7}Li SLR NMR rates were measured with the saturation recovery technique. A comb of closely spaced 90° pulses destroys the longitudinal magnetization; subsequently, its recovery is probed as a function of delay time with a single (90°) detection pulse.[53]

^{7}Li NMR spin-alignment echoes were monitored by means of the Jeener–Broekaert pulse sequence[16,54,55] $90°_X - t_p - 45°_Y - t_m - 45°_\delta - t_{acqu}$. The 90° pulse length was 3 μs. The preparation time t_p has to be chosen as short as possible,[12,56,57] here t_p = 10 μs to suppress dipolar contributions to the quadrupolar spin-alignment echo. The mixing time t_m was varied from 10 μs to 10 s. A 32-fold phase cycling[55] was used to pick out the desired coherence pathway. Up to 128 scans were used to sample NMR spin-alignment echoes as a function of mixing time but with constant preparation time. The recycle delay between each scan was at least $5T_1$. The final temperature-dependent two-time correlation functions were obtained by plotting the echo intensity S_2 as a function of t_m in a semi-logarithmic representation.

2.2 Impedance spectroscopy

Impedance spectroscopy measurements on cold-pressed polycrystalline samples with Au electrodes (see above) were carried out with an HP 4192 A analyzer as well as a Novocontrol Concept 80 broadband dielectric spectrometer. The HP impedance analyzer, working at frequencies from 5 Hz to 13 MHz, is connected to a home-built cell which allows measurements under inert gas atmosphere, here dry nitrogen gas (99.999%). The temperature in the cell was adjusted and monitored with a Eurotherm controller. The Concept 80 impedance analyzer is equipped with a BDS 1200 cell and an Alpha analyzer which is capable of measuring conductances down to 10^{-14} S at frequencies ranging from a few μHz to 20 MHz. Temperature regulation and control within an accuracy of about 0.5 K was carried out with a Quatro cryosystem (Novocontrol) using freshly evaporated nitrogen.

3 Results and discussion

Li diffusion in polycrystalline β-Li_2TiO_3 was investigated by both temperature-variable ^{7}Li SAE NMR spectroscopy (165–500 K) and ac-conductivity measurements (240–835 K). The structure refinement by Kataoka *et al.*[58] envisaged Li_2TiO_3 as a distorted rocksalt structure with alternating Li and LiT_2 (111) planes described with the $C2/c$ space group (see Fig. 1). Regarding $C2/c$ symmetry all of the Li cations reside in octahedral sites in β-Li_2TiO_3.[34] While the two magnetically inequivalent positions 8f and 4d in the pure Li-layer are fully occupied by lithium cations (Li(1) and Li(2)), Ti and the residual Li ions, Li(3), share the 4e position in the $LiTi_2$ layers being characterized by two crystallographically inequivalent titanium sites Ti(1) and Ti(2). Each $LiTi_2$ plane can be described as a honeycomb structure with six Ti ions creating a hexagon centered on a Li ion. Finally, a complex stacking sequence of the $LiTi_2$ layers results in a glide plane and the $C2/c$ space group.[59] At higher temperatures (>970 K) different (more simple) stacking sequences of the $LiTi_2$ planes are reported[60] leading to short-range regimes crystallizing, besides $C2/c$, with the space groups $C2/m$ and $P3_112$ showing three (2b, 2c, 4h) and four (3b, 3a) inequivalent Li positions, respectively.[59] Note, if Ti and Li are randomly distributed among the positions within a $LiTi_2$ layer, the number of electrically inequivalent Li sites is additionally increased. Hence, irrespective of the actual symmetry of β-Li_2TiO_3, the oxide provides distinct

View Article Online

Published on 03 July 2012. Downloaded by Technische Informationsbibliothek (TIB) on 26/10/2017 14:16:50.

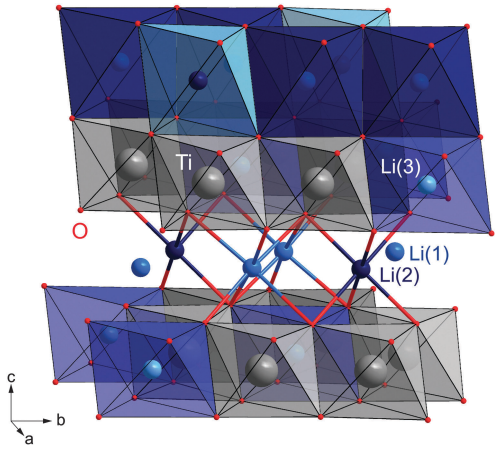

Fig. 1 Crystal structure of β-Li_2TiO_3. Each crystallographically inequivalent Li site i, either located within (Li(3)) or between (Li(1), Li(2)) the LiT_2 layers is characterized by a specific quadrupole frequency $\omega_{Q,i}$. While hopping from site to site a Li ion experiences a series of different electric field gradients; the associated fluctuations of the quadrupole frequencies per unit of time can be used to estimate the Li jump rate. Depending on the stacking sequence of the $LiTi_2$ layers up to four crystallographically, and thus electrically, inequivalent Li sites do exist. Additionally, the random distribution of Li and Ti cations within the layers is anticipated to lead to various magnetically inequivalent Li sites.

magnetically, and thus electrically, inequivalent Li sites characterized by individual (site-specific) NMR resonance frequencies. During Li diffusion the associated temporal changes in the corresponding NMR (quadrupole) frequencies, ω_Q, the ions experience can be used to directly record Li jump rates at different temperatures by ^{7}Li SAE NMR.

3.1 ^{7}Li SAE NMR spectroscopy

The site-specific quadruple frequencies $\omega_{Q,i}$ are determined by the orientation of the external magnetic field with respect to the quadrupole coupling tensor. The tensor quantifies the interaction of the quadrupole moment of the ^{7}Li nucleus (spin-quantum number $I = 3/2$) with a non-vanishing, site-dependent electric field gradient. Hopping of the Li ions between electrically distinct positions renders ω_Q time-dependent which allows the acquisition of a (two-time) motional correlation function reflecting the changes in $\omega_{Q,i}$ as a function of observation (or mixing) time t_m. This (single-spin) correlation function, which is given by the NMR spin-alignment echo height S_2 *vs.* t_m, contains the information about the probability of finding a spin, which was exposed to ω_Q at $t' = 0$, in the same state, *i.e.*, exposed to the same quadrupole frequency, at a later time $t' = t_m$.[16–19,23,25,52,56,57]

In many cases S_2, which is here given by

$$S_2(t_p, t_m) = \frac{9}{20}\langle \sin[\omega_Q(t_m = 0)t_p]\sin[\omega_Q(t_m)t_p]\rangle \qquad (1)$$

follows a stretched exponential from which the decay rate $\tau_{SAE}^{-1} = f(T)$, being in the ideal case very similar to the (mean) Li jump rate τ^{-1}, can easily be determined by appropriate parameterizing with the Kohlrausch–Williams–Watts (KWW) function.[61,62]

$$S_2(t_p,t_m) \propto \exp(-(t_m/\tau_{SAE})^{\gamma_\varepsilon}) \qquad (2)$$

The so-called 'sin–sin' correlation function S_2 was recorded[16] by utilizing the Jeener–Broekaert sequence[54] mentioned above. The short evolution period determined by $t_p \ll \tau$ is followed by the mixing period ranging from $t_m = 10$ μs to $t_m = 10$ s. Here, taking into account receiver dead time effects and those related to mistimed echo generation,[63] the echo maximum shows up at $t' = t_p + 8$ μs. In the present case, echo intensities were always read out at $t = t'$.

In Fig. 2(A) and (B) the so obtained Li decay rates τ_{SAE}^{-1} and the corresponding ^{7}Li SAE NMR two-time correlation functions $S_2(t_p = 10\ \mu s, t_m, t = t_p)$ of β-Li_2TiO_3 are shown. The first are shown in Fig. 2(A) in an Arrhenius plot together

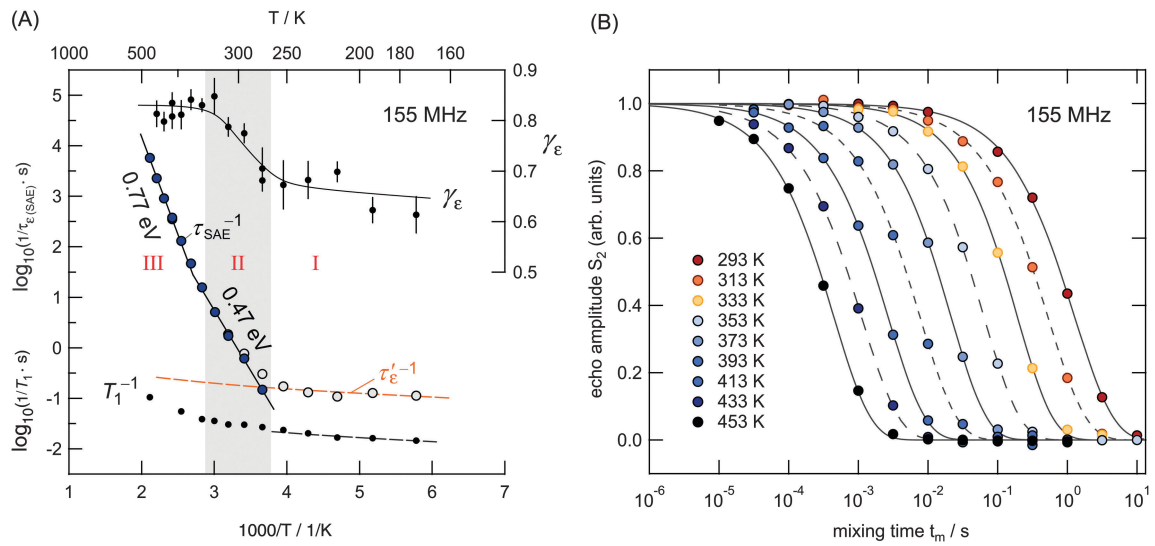

Fig. 2 (A) Arrhenius plot of τ_{SAE}^{-1} obtained from analyzing the ^{7}Li SAE NMR two-time correlation functions $S_2(t_p = 10\ \mu s, t_m, t = t_p)$ of β-Li_2TiO_3. (B) The S_2 curves were parameterized by stretched exponentials (*cf.* eqn (2)) containing τ_{SAE}^{-1} and γ_ε. ^{7}Li NMR SLR rates (T_1^{-1}) are shown as well for comparison with the SAE NMR decay rates. For the sake of brevity, the curves recorded at $T > 293$ K are not included. The echo amplitudes S_2 shown as a function of mixing time t_m are scaled such that they range from 1 to 0. See text for further explanation.

 This journal is © the Owner Societies 2012

View Article Online

Published on 03 July 2012. Downloaded by Technische Informationsbibliothek (TIB) on 26/10/2017 14:16:50.

with the independently measured ^{7}Li NMR SLR rates T_1^{-1}. For comparison with the temperature dependence of τ_{SAE}, the stretching exponents $\gamma_\varepsilon = f(T)$ are also included. Fits according to eqn (2) are shown as dashed and solid lines in Fig. 2(B).

As expected the echo decay curves in Fig. 2(B) shift to shorter mixing times with increasing temperature indicating the influence of Li diffusion on echo damping. As can be seen in Fig. 2(A) the temperature dependence of τ_{SAE}^{-1} can be subdivided into three regimes: I, II, and III. At low temperatures ($T < 250$ K, regime I) the decay rates are almost independent of T (grey circles in Fig. 2(A)). Most likely, τ_{SAE}^{-1} reflects the influence of spin-diffusion and/or spin–lattice relaxation on echo decay. In this regime the exact temperature dependence of the rates can be well represented by a power law, $\tau_{SAE}^{-1} = \tau_\varepsilon'^{-1} \propto T^\alpha$, which resembles that of the corresponding T_1^{-1} rates (see dashed lines in Fig. 2(A)). Here, below 250 K the rates T_1^{-1} are given by $T_1^{-1} \approx 1/8 \times \tau_\varepsilon'^{-1}$.

With increasing temperature, S_2 is increasingly influenced by Li diffusion resulting in a significant temperature dependence of τ_{SAE}^{-1} (regime II). In order to take into account the influence of the background contribution in this transition regime, the low-T rates $\tau_\varepsilon'^{-1}$ have been extrapolated to higher temperatures and subtracted from the measured τ_{SAE}^{-1} data (see full circles in Fig. 2(A)). In regime II (365 K $> T >$ 265 K) τ_{SAE}^{-1} follows an Arrhenius law, $\tau_{SAE}^{-1} = \tau_{0,SAE}^{-1} \exp(-E_{a,SAE}/(k_B T))$, with an activation energy of $E_{a,SAE} = 0.47(2)$ eV (k_B denotes Boltzmann's constant).

At even higher temperatures ($T >$ 370 K, regime III) the influence of $\tau_\varepsilon'^{-1}$ on τ_{SAE} becomes negligible and the SAE NMR decay rate is solely induced by Li diffusion. The corresponding activation energy $E_{a,SAE}$ is increased from 0.47(2) eV to 0.77(2) eV. The pre-exponential factor $\tau_{0,SAE}^{-1}$ turned out to be in the order of 10^{12} s^{-1}. Most likely, the diffusion process showing up in regime III reflects hopping of the Li ions between all crystallographic sites available, *i.e.*, jump processes between the sites Li(1) and Li(2) in the *ab*-plane as well as Li hopping perpendicular to the $LiTi_2$-layers by involving the Li(3) sites.

As can be clearly seen in Fig. 2(A) the slow dynamic process revealed by ^{7}Li SAE NMR in regime III cannot be detected by SLR NMR in the temperature range covered. Even at temperatures up to 500 K the corresponding T_1^{-1} rates are mainly governed by a non-diffusive background contribution. While SAE NMR is sensitive to extremely slow Li motions, with the help of SLR NMR much faster Li jump processes can be probed. Here, the so-called NMR SLR rate peak is expected to show up at much higher T. In general, the SLR NMR rates will pass through a maximum when the mean Li jump rate τ^{-1} reaches the order of the Larmor frequency, *i.e.*, when $\tau^{-1} \approx 10^9$ s^{-1}. Similar holds true for SLR_ρ NMR measurements performed in the rotating frame of reference, *i.e.*, at locking frequencies in the kHz range. The corresponding peaks $T_{1\rho}^{-1}$ ($1/T$) show up when $\tau^{-1} \approx 5 \times 10^5$ s^{-1}, which, in the present case, is expected to be at $T >$ 500 K. Indeed this is found by preliminary SLR_ρ NMR measurements.[64]

Interestingly, the different regimes observed for τ_{SAE} are also reflected by the temperature dependence of γ_ε. In the low-temperature regime, $\gamma_\varepsilon (\approx 0.65)$ turns out to depend only slightly on T, while in the transition regime (II) the stretching exponent becomes temperature dependent and increases from 0.65 to 0.82, which is the value being finally reached in regime III. Note that preliminary SLR_ρ NMR measurements performed in the rotating frame of reference at locking frequencies in the order of some kHz also point to non-exponential motional correlation functions.[64] In many cases deviations from single exponential behaviour might be attributed to a distribution of jump rates.[20,24,51] Here, a γ_ε value of 0.82 indicates a rather small distribution width as could be expected for a highly ordered crystal structure with a regularly shaped potential landscape. For comparison, amorphous materials such as glasses in many cases reveal stretching exponents γ_ε of 0.3 and less, which is typical for highly heterogeneous dynamics.[20,24,51,66,67]

The SAE NMR decay rates τ_{SAE}^{-1} can be transformed into (self-)diffusion coefficients D_{SAE} by using the Einstein–Smoluchowski equation[68]

$$D_{SAE} = a^2/(2d\tau_{SAE}). \quad (3)$$

Assuming three-dimensional diffusion ($d = 3$) and a jump distance of approximately 0.29 nm, which is based on the crystal structure refinement of Kataoka *et al.*,[58] results in $D_{SAE} \approx 2 \times 10^{-17}$ m^2 s^{-1} at 433 K.

3.2 Impedance measurements

Interestingly, a very similar value for the diffusion coefficient can be deduced from IS measurements. In Fig. 3(A) so-called charge diffusivities are shown which were obtained by converting dc conductivity values into diffusion coefficients D_σ with the help of the Nernst–Einstein equation.[68]

$$D_\sigma = \frac{\sigma_{dc} k_B T}{N q^2} \quad (4)$$

where q represents the charge of the Li ions and N denotes the number density of charge carriers. σ_{dc} was determined from the frequency independent plateaus of the impedance spectra $\sigma'(\nu)$ shown in Fig. 3(B). Here, the dc conductivity σ_{dc} was identified with the real part σ' of the complex conductivity in the frequency regime where $\sigma' \neq f(\nu)$. In the present case, σ_{dc}, *i.e.*, $\sigma'(\nu \to 0)$, could be accurately determined since the conductivity isotherms show well-defined dc plateaus which have here been identified with a transport process in the bulk of β-Li_2TiO_3. At higher frequencies ν the plateaus pass over into dispersive regimes,[69] which roughly follow a power law behaviour $\sigma' = \sigma_{dc} + A\nu^s$. A and s represent two fitting parameters.[69] In the case of three-dimensional diffusion (see above) s usually ranges from 0.5 to 0.8. Here, at $T = 243$ K being the lowest temperature accessible with our equipment, $s \approx 0.64$. The drop in σ' showing up at low frequencies and high temperatures (>400 K, Fig. 3(B)) can simply be ascribed to polarization effects of the ion-blocking electrodes used. As an example, D_σ turns out to be in the order of 10^{-17} m^2 s^{-1} at 433 K (see Fig. 3(A) (right-hand axis)). This is in very good agreement with the value probed by SAE NMR (see above).

In general, the two diffusion coefficients D_σ and D_{SAE} are related to the macroscopic tracer diffusion coefficient D_{tr} according to $D_\sigma = D_{tr}/H_R$ and $D_{SAE} = D_{tr}/f$, *i.e.*, $D_{SAE}/D_\sigma = H_R/f$. Here, H_R denotes the Haven ratio and f is the correlation factor reflecting the degree of correlated motion present. It ranges

View Article Online

Published on 03 July 2012. Downloaded by Technische Informationsbibliothek (TIB) on 26/10/2017 14:16:50.

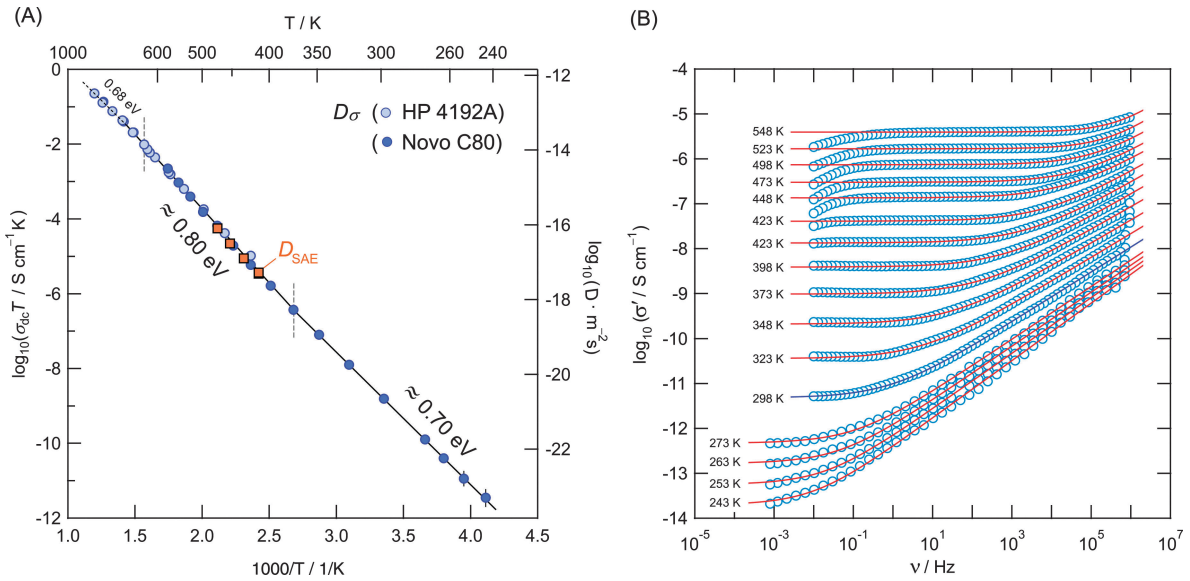

Fig. 3 (A) Arrhenius plot of the Li solid-state diffusion coefficients D_σ (see right axis) of Li_2TiO_3 as derived, according to eqn (4), from the σ_{dc} values which were measured by IS (see Sections 2.2 and 3.2 for further details).[65] Note, the left axis shows the corresponding $\sigma_{dc}T$ values which were determined from the conductivity isotherms ($\sigma'(\nu)$) shown in (B). Because of $D_\sigma \propto \sigma_{dc}T$ the respective Arrhenius lines are characterized by the same slopes. Solid lines in (B) show fits with appropriate power laws.

between 0 and 1; $f = 1$ is obtained for uncorrelated motion. The good agreement found between D_σ and D_{SAE} (see Fig. 3(A)) indicates that H_R/f is close to one. Note that for comparison, in Fig. 3(A) four D_{SAE} values have been included which were measured at the highest temperatures of regime III (see Fig. 2(A)). The activation energies indicated in Fig. 3(A) were obtained by fitting the data according to

$$D_\sigma \propto \exp(-E_{a,dc}/(k_B T)). \quad (5)$$

In the range from 380 K to 700 K the fit yields $E_{a,dc} = 0.80(1)$ eV which is in perfect agreement with the value solely deduced from SAE NMR (0.77(2) eV).[70] Since σ_{dc}, and thus D_σ, is sensitive to successful ion jumps leading to macroscopic transport, the good agreement of D_σ with D_{SAE} clearly demonstrates that with SAE NMR long-range ion dynamics can be probed. Recently, this similarity has been shown for several crystalline and amorphous materials, respectively.[8,71] Obviously, in regime III both SAE NMR and dc-conductivity measurements are sensitive to very similar motional correlation functions.

However, in regime II the two methods reveal significant differences when both the absolute values of the respective diffusion coefficients and the associated activation energies (0.47 eV *vs.* 0.77 eV) are considered. It is noteworthy that below 270 K the dc plateau is largely shifted towards lower frequencies making the accurate determination of σ_{dc} difficult. On the other hand, τ_{SAE}^{-1} is increasingly influenced by non-diffusive background effects. Nevertheless, one might consider that the low-T rates τ_{SAE}^{-1} determined in regime II might also be influenced (i) by diffusion-induced SLR in the dipolar field of the ^{7}Li spins or (ii) by short-range Li dynamics taking place in Li_2TiO_3 to which σ_{dc} is not sensitive. Whilst the first effect may be ruled out by ^{6}Li SAE NMR measurements, the latter influence can be examined by determining $\sigma'(\nu)T$ at frequencies of the order of 10^4 to 10^5 s^{-1}. Indeed, when, *e.g.*, $\sigma'(\nu)T$ is read out at $\nu = 10^4$ s^{-1} and plotted *vs.* the inverse temperature an activation energy $E_{a,ac}$ of only 0.37(2) eV (300–400 K) is found. A very similar ac activation energy (0.36(2) eV) is obtained at $\nu = 10^5$ s^{-1}. The corresponding power law exponents s range from 0.55 (300 K) to 0.51 (400 K). Interestingly, using a mean value $\bar{s}$ of 0.53, in regime II the relation $E_{a,ac} + (1 - \bar{s})E_{a,dc}$ roughly holds[72–74] when 0.80 eV is inserted for $E_{a,dc}$.[75] One might speculate whether the diffusion process of regime II reflects localized Li hops[69] in the *ab*-plane, *i.e.*, between the $LiTi_2$ layers in Li_2TiO_3.

Finally, at this point let us compare our results with those recently presented by Vijayakumar *et al.*[49] having recorded SAE NMR decay curves up to $T = 365$ K, that is, in regime II only. As compared to our findings they reported an activation energy $E_{a,SAE}$ of 0.27(4) eV. The recently published data seem to suffer from rather large non-diffusive background rates $\tau_\varepsilon'^{-1}$. Usually, this indicates a less pure sample since the background decay rates are largely influenced by coupling of the spins to paramagnetic impurities. Unfortunately, the low-T decay rates have not been used to correct the diffusion-induced SAE NMR rates τ_{SAE}^{-1} showing up above 285 K, *cf.* also the correction procedure introduced by Vogel and co-workers.[51] Taken together this easily leads to a smaller slope and thus to an apparently lower activation energy than found here. Certainly, as already pointed out by Vijayakumar *et al.*,[49] impurities and deviations from ideal stoichiometry, in general, are expected to lower E_a in addition. Thus, the exact defect chemistry introduced during preparation of the samples seems to largely influence the short-range ion dynamics on the titanate studied.

4 Conclusions

^{7}Li SAE NMR spectroscopy was used to measure extremely low Li jump rates in a polycrystalline, highly pure sample of

 This journal is © the Owner Societies 2012

View Article Online

Published on 03 July 2012. Downloaded by Technische Informationsbibliothek (TIB) on 26/10/2017 14:16:50.

monoclinic metatitanate Li_2TiO_3. Parameterizing the NMR two-time single particle correlation functions with stretched exponentials results in decay rates ranging from 10^{-1} to 10^4 s^{-1}. Above 370 K the rates are consistent with results from impedance spectroscopy measurements pointing to long-range Li transport being characterized with an activation energy of approximately 0.8 eV. In conclusion, this shows that ^{7}Li SAE NMR spectroscopy, being an atomic-scale method, gives access to long-range Li transport in solids which is crucial for the development of advanced energy storage materials such as electrodes and electrolytes. Interestingly, at lower temperatures a jump process with an activation energy of only 0.47 eV shows up which might be ascribed to Li jump processes taking place on a shorter length scale. These might also involve Li jumps within the *ab*-plane of monoclinic Li_2TiO_3.

Acknowledgements

Financial support from the Deutsche Forschungsgemeinschaft (DFG) within the frame of the Research Unit 1277 (DFG-Forschergruppe 1277) "Mobilität von Lithium-Ionen in Festkörpern" is gratefully acknowledged.

References

1 J.-M. Tarascon and M. Armand, *Nature*, 2001, **1414**, 359.
2 M. Armand and J.-M. Tarascon, *Nature*, 2008, **451**, 652.
3 J.-M. Tarascon, *ChemSusChem*, 2008, **1**, 777.
4 A. S. Aricó, P. Bruce, B. Scrosati, J.-M. Tarascon and W. V. Schalkwijc, *Nat. Mater.*, 2005, **4**, 366.
5 P. G. Bruce, B. Scrosati and J.-M. Tarascon, *Angew. Chem., Int. Ed.*, 2008, **47**, 2930.
6 Z. Yang, J. Zhang, M. C. W. Kintner-Meyer, X. Lu, D. Choi, J. P. Lemmon and J. Liu, *Chem. Rev.*, 2011, **111**, 3577.
7 P. Heitjans and S. Indris, *J. Phys.: Condens. Matter*, 2003, **15**, R1257.
8 M. Wilkening and P. Heitjans, *ChemPhysChem*, 2012, **13**, 53.
9 D. L. Sidebottom, *Rev. Mod. Phys.*, 2009, **81**, 999.
10 K. Funke, C. Cramer and D. Wilmer, *Diffusion in Condensed Matter – Methods, Materials, Models*, Springer, Berlin, 2nd edn, 2005, ch. 21, pp. 857–893.
11 K. L. Ngai, *Relaxation and Diffusion in Complex Systems*, Springer, New York, 2011.
12 R. Böhmer, T. Jörg, F. Qi and A. Titze, *Chem. Phys. Lett.*, 2000, **316**, 419.
13 M. Wilkening and P. Heitjans, *Defect Diffus. Forum*, 2005, **237–240**, 1182.
14 F. Qi, G. Diezemann, H. Böhm, J. Lambert and R. Böhmer, *J. Magn. Reson.*, 2004, **169**, 225.
15 F. Qi, C. Rier, R. Böhmer, W. Franke and P. Heitjans, *Phys. Rev. B: Condens. Matter Mater. Phys.*, 2005, **72**, 104301.
16 R. Böhmer, K. Jeffrey and M. Vogel, *Prog. Nucl. Magn. Reson. Spectrosc.*, 2007, **50**, 87.
17 R. Böhmer and F. Qi, *Solid State Nucl. Magn. Reson.*, 2007, **31**, 28.
18 B. Koch and M. Vogel, *Solid State Nucl. Magn. Reson.*, 2008, **34**, 37.
19 S. Faske, B. Koch, S. Murawski, R. Kuechler, R. Boehmer, J. Melchior and M. Vogel, *Phys. Rev. B: Condens. Matter Mater. Phys.*, 2011, **84**, 024202.
20 C. Brinkmann, S. Faske, B. Koch and M. Vogel, *Z. Phys. Chem.*, 2010, **224**, 1535.
21 M. Wilkening, W. Küchler and P. Heitjans, *Phys. Rev. Lett.*, 2006, **97**, 065901.
22 M. Wilkening, D. Gebauer and P. Heitjans, *J. Phys.: Condens. Matter*, 2008, **20**, 022201.
23 M. Wilkening and P. Heitjans, *Phys. Rev. B: Condens. Matter Mater. Phys.*, 2008, **77**, 024311.
24 M. Wilkening, A. Kuhn and P. Heitjans, *Phys. Rev. B: Condens. Matter Mater. Phys.*, 2008, **78**, 054303.
25 M. Wilkening and P. Heitjans, *J. Phys.: Condens. Matter*, 2006, **18**, 9849.
26 M. Wilkening, R. Amade, W. Iwaniak and P. Heitjans, *Phys. Chem. Chem. Phys.*, 2006, **9**, 1239.
27 M. Wilkening and P. Heitjans, *Solid State Ionics*, 2006, **177**, 3031.
28 M. Wilkening, C. Mühle, M. Jansen and P. Heitjans, *J. Phys. Chem. B*, 2007, **111**, 8691.
29 H. W. Spiess, *J. Chem. Phys.*, 1980, **72**, 6755.
30 M. Lausch and H. W. Spiess, *J. Magn. Reson.*, 1983, **54**, 466.
31 F. Fujara, S. Wefing and H. Spiess, *J. Chem. Phys.*, 1986, **84**, 4579.
32 T. Dries, F. Fujara, M. Kiebel, E. Rössler and H. Silescu, *J. Chem. Phys.*, 1988, **88**, 2139.
33 G. Fleischer and F. Fujara, in *NMR—Basic Principles and Progress*, Springer, Berlin, 1994, vol. 30.
34 J. Dorrian and R. Newnham, *Mater. Res. Bull.*, 1969, **4**, 179.
35 G. Izquierdo and A. West, *Mater. Res. Bull.*, 1980, **15**, 1655.
36 J. Mikkelsen, *J. Am. Ceram. Soc.*, 1980, **63**, 331.
37 C. Johnson, J. Kim, A. Kropf, A. Kahaian, J. Vaughey and M. Thackeray, *J. Power Sources*, 2003, **119**, 139.
38 L. Zhang, K. Takada, N. Ohta, M. Osada and T. Sasaki, *J. Power Sources*, 2007, **174**, 1007.
39 C. Alvani, S. Casadio, V. Contini, A. D. Bartolomeo, J. Lulewicz and N. Roux, *J. Nucl. Mater.*, 2002, **307–311**, 837.
40 A. R. Raffray, M. Akiba, V. Chuyanov, L. Giancarli and S. Malang, *J. Nucl. Mater.*, 2002, **307**, 21.
41 J. van der Laan, H. Kawamura, N. Roux and D. Yamaki, *J. Nucl. Mater.*, 2000, **283**, 99.
42 J. Kopasz, J. Miller and C. Johnson, *J. Nucl. Mater.*, 1994, **212–215**, 927.
43 N. Roux, J. Avon, A. Floreancing, J. Mougin, B. Rasneur and S. Ravel, *J. Nucl. Mater.*, 1996, **233–237**, 1431.
44 H. Kleykamp, *J. Nucl. Mater.*, 2001, **295**, 244.
45 C. Gicquel, M. Mayer and R. Bouaziz, *Compt. Rend. (Paris) Ser. C*, 1972, **275**, 1427.
46 T. Fehr and E. Schmidbauer, *Solid State Ionics*, 2007, **178**, 35.
47 This value, reported by Fehr *et al.*,[46] is in very good agreement with that one deduced by the conductivity measurements presented here, which is 4×10^{-6} S cm^{-1}, see Fig. 2(A).
48 Ģ. Vītiņš, G. Ķizāne, A. Lūsis and J. Tīliks, *J. Solid State Electrochem.*, 2002, **6**, 311.
49 M. Vijayakumar, S. Kerisit, Z. Yang, G. L. Graff, J. Liu, J. A. Sears and S. D. Burton, *J. Phys. Chem. C*, 2009, **113**, 20108.
50 P. Heitjans, A. Schirmer and S. Indris, in *Diffusion in Condensed Matter – Methods, Materials, Models*, Springer, Berlin, 2nd edn, 2005, ch. 9, pp. 369–415.
51 S. Faske, H. Eckert and M. Vogel, *Phys. Rev. B: Condens. Matter Mater. Phys.*, 2008, **77**, 104301.
52 M. Wilkening, J. Heine, C. Lyness, A. R. Armstrong and P. G. Bruce, *Phys. Rev. B: Condens. Matter Mater. Phys.*, 2009, **80**, 064302.
53 E. Fukushima and S. Roeder, *Experimental Pulse NMR*, Addison-Wesley, Reading, 1981.
54 J. Jeener and P. Broekaert, *Phys. Rev.*, 1967, **157**, 232.
55 R. Böhmer, *J. Magn. Reson.*, 2000, **147**, 78.
56 X.-P. Tang and Y. Wu, *J. Magn. Reson.*, 1998, **133**, 155.
57 F. Qi, T. Jörg and R. Böhmer, *Solid State Nucl. Magn. Reson.*, 2002, **22**, 484.
58 K. Kataoka, Y. Takahashi, N. Kijima, H. Nagai, J. Akimoto, Y. Idemoto and K. Ohshima, *Mater. Res. Bull.*, 2009, **44**, 168.
59 S. T. Murphy, P. Zeller, A. Chartier and L. V. Brutzel, *J. Phys. Chem. C*, 2011, **115**, 21874.
60 N. V. Tarakina, R. B. Neder, T. A. Denisova, L. G. Maksimova, Y. V. Baklanova, A. P. Tyutyunnik and V. G. Zubkov, *Dalton Trans.*, 2010, **39**, 8168.
61 R. Kohlrausch, *Pogg. Annu. Phys. Chem.*, 1854, **91**, 179.
62 F. Williams and D. C. Watts, *Trans. Faraday Soc.*, 1970, **66**, 80.
63 R. Böhmer, S. Faske and B. Geil, *Solid State Nucl. Magn. Reson.*, 2008, **34**, 32.
64 B. Ruprecht, PhD thesis, Leibniz University Hannover, 2012, unpublished results.
65 It is noteworthy that the σ_{dc} values recorded do not reveal significant deviations from an Arrhenius line indicating, for example, pronounced structural changes of Li_2TiO_3 in the temperature range covered here.

View Article Online

However, above 700 K the ion conductivity σ_{dc} seems to follow an Arrhenius law characterized by a somewhat smaller activation energy of only 0.68 eV (see dashed line in Fig. 3(A)).
66 M. Vogel, C. Brinkmann, H. Eckert and A. Heuer, *Phys. Rev. B: Condens. Matter Mater. Phys.*, 2004, **69**, 094302.
67 M. Vogel, C. Brinkmann, H. Eckert and A. Heuer, *J. Non-Cryst. Solids*, 2006, **352**, 5156.
68 H. Mehrer, *Diffusion in Solids.*, Springer, Berlin, 2006.
69 Interestingly, at intermediate temperatures the dispersive regime reveals a slight shoulder, see, *e.g.*, the data points near $\nu = 10\ s^{-1}$ of the isotherm recorded at 323 K. This feature might also be related to some localized hopping processes in Li_2TiO_3.
70 Disregarding the slight changes in slope of the $\sigma_{dc}T$ values plotted in Fig. 3(A), a single (overall) Arrhenius fit (250 K to 900 K) yields 0.75 eV.[64]
71 B. Ruprecht, H. Billetter, U. Ruschewitz and M. Wilkening, *J. Phys.: Condens. Matter*, 2010, **22**, 245901.
72 K. L. Ngai and O. Kanert, *Solid State Ionics*, 1992, **53–56**, 936.
73 K. L. Ngai and S. W. Martin, *Phys. Rev. B: Condens. Matter Mater. Phys.*, 1989, **40**, 10550.
74 K. L. Ngai, G. N. Greaves and C. T. Moynihan, *Phys. Rev. Lett.*, 1998, **80**, 1018.
75 Note that *s* increases to 0.64 when *T* is decreased to 243 K. Above 500 K another increase of *s* is found reaching 0.68 at 573 K.

Published on 03 July 2012. Downloaded by Technische Informationsbibliothek (TIB) on 26/10/2017 14:16:50.

This journal is © the Owner Societies 2012